

This is a repository copy of *Controlling X-Ray Flux in Hohlraums Using Burn-through Barriers*.

White Rose Research Online URL for this paper:

<https://eprints.whiterose.ac.uk/166272/>

Version: Accepted Version

Article:

Trickey, William, Owen, Joseph, Ridgers, Christopher Paul orcid.org/0000-0002-4078-0887 et al. (1 more author) (2020) Controlling X-Ray Flux in Hohlraums Using Burn-through Barriers. *Physics of Plasmas*. 103301. ISSN 1089-7674

<https://doi.org/10.1063/5.0014798>

Reuse

Items deposited in White Rose Research Online are protected by copyright, with all rights reserved unless indicated otherwise. They may be downloaded and/or printed for private study, or other acts as permitted by national copyright laws. The publisher or other rights holders may allow further reproduction and re-use of the full text version. This is indicated by the licence information on the White Rose Research Online record for the item.

Takedown

If you consider content in White Rose Research Online to be in breach of UK law, please notify us by emailing eprints@whiterose.ac.uk including the URL of the record and the reason for the withdrawal request.

Controlling X-Ray Flux in Hohlräume Using Burn-through Barriers

William Trickey,¹ Joseph Owen,¹ Christopher Ridgers,¹ and John Pasley^{*1}

¹*York Plasma Institute, University of York, Heslington, York YO10 5DQ, United Kingdom*

^{*} *Corresponding author. Email: john.pasley@york.ac.uk*

A technique for controlling X-ray flux in hohlraums is presented. In Indirect Drive Inertial Confinement Fusion (ICF) the soft X-rays arriving at the spherical fuel capsule are required to have a specific temporal profile and high spatial uniformity in order to adequately compress and ignite the fuel. Conventionally this is achieved by modifying the external driver, the hohlraum geometry, and the sites of interaction between the two. In this study a technique is demonstrated which may have utility in a number of scenarios, both related to ICF and otherwise, in which precise control over the X-ray flux and spatial uniformity are required. X-ray burn-through barriers situated within the hohlraum are shown to enable control of the flux flowing to an X-ray driven target. Control is achieved through the design of the barrier rather than by modification of the external driver. The concept is investigated using the one-dimensional (1-D) radiation hydrodynamics code HYADES in combination with a three-dimensional (3-D) time-dependent viewfactor code.

INTRODUCTION

In indirect drive ICF the implosion of a fusion fuel capsule is driven by a bath of soft X-rays. The incident X-ray flux vs. time profile must be precisely controlled in order to launch a series of appropriately timed shocks into the capsule [1]. Additionally, a high spatial uniformity must be maintained in order to minimise low-mode asymmetries that would otherwise degrade the implosion [2–4]. The drive X-rays are produced via the heating of a hohlraum surrounding the capsule. This heating may in principle be achieved using either laser beams, pulsed-power sources or ion-beams. The characteristics of the X-rays that are incident at the capsule surface are managed through modification of the hohlraum geometry, the properties of the drivers, and the location(s) at which the driver energy interacts with the hohlraum. For example, laser-driven indirect drive ICF uses temporally-shaped laser pulses that are incident on the interior of the hohlraum at locations designed to produce optimal spherical uniformity of the X-ray drive at the capsule surface. In addition to ICF there are also a range of other types of high energy density (HED) physics experiments that require precise control of the x-ray flux reaching the surface of a target [5–11]. Here we demonstrate a technique for modifying the X-rays incident upon such targets using burn-through barriers.

Historically a large amount of work has been performed to investigate the interaction between high intensity lasers and thin, high atomic-number (high-Z) foils with the objective of producing X-ray sources [12–17]. These components are typically referred to as burn-through foils, and are commonly employed in HEDP experiments for back-lighting purposes; this is a different concept from that which is described here. In this study we consider barriers that modulate the flow of X-ray radiation from one region of a hohlraum to another; the energy of the external driver is not incident directly upon the barrier. Previous work on X-ray burn-through has been

focussed on ablator preheat [18] and hohlraum wall re-emission [19]. Here an application of X-ray burn-through is demonstrated in which it is used to modify the flow of X-rays within a hohlraum in order to modify the X-ray radiation field driving a target. It is shown that use of such a barrier can significantly alter the properties of the X-rays reaching the target, changing both their temporal and spatial characteristics. Facilities that are able to create high intensity X-ray sources for heating matter to HED conditions may be limited in their control over the spatial and temporal properties of the source. For example, most laser facilities have limited pulse-shaping capabilities and the number of beams available may not be sufficient to produce the X-ray illumination uniformity required by certain targets. The burn-through barrier technique described here could be used to modify the flow of x-rays to the intended target, thereby rendering them better suited to a given application. Figure 1 shows an illustration of the hohlraum burn-through barrier concept. The chamber in which the external source deposits its energy is blocked-off from the hohlraum interior; the barrier can be designed so as to hold back the radiation and then burn-through rapidly, leading to a fast rising radiation temperature in the interior which is largely independent of the temporal properties of the external driver. A more complex barrier can enable more sophisticated temporal pulse shaping. By changing the composition of the barrier in the radial direction, the spatial characteristics of the X-ray drive can also be modified.

The configuration described here is somewhat similar to that of the multi-chamber hohlraums proposed previously [20–22].

The use of burn-through barriers in combination with more conventional hohlraum design techniques may help address a number of issues. Z-pinch driven hohlraums are capable of producing large X-ray fluxes [22–24], however temporal pulse shaping is difficult and requires complex nested z-pinch arrays [24, 25]. Spatially, modifi-

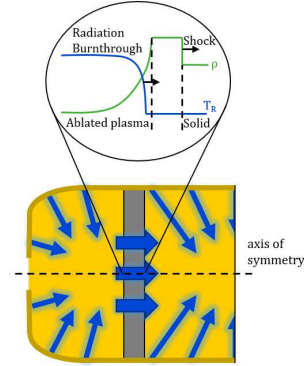


FIG. 1: A diagram that shows the cross section of one half of a burn-through barrier hohlraum. Radiation builds up in the external chamber (left) and will burn through to the main chamber (right).

cation of the drive profile is limited to power balancing of the secondary hohlraums and the target geometry [24]. Burn-through barriers could be placed between the primary and secondary hohlraum chambers, enabling greater control over both temporal and spatial characteristics of the drive. There also remain some outstanding issues in regard to laser driven hohlraums, even at facilities as sophisticated as the National Ignition Facility [26]. Hotspots are created at the laser absorption sites which can cause X-ray drive asymmetries [3, 4] as well as fuel pre-heat due to M-band [27] emission. Further to this, at late stages of ICF implosions laser-plasma interactions occur in the plasma fill that reduce the laser to X-ray conversion efficiency and creates significant populations of suprathermal electrons [28–30]. A burn-through barrier may provide some degree of shielding between the laser interaction region and the target, though it is outside the scope of the present manuscript to investigate this application. There is also an appreciable time-lag in the rise in the X-ray flux relative to any increase in the laser drive intensity, making it difficult to produce sudden jumps in the X-ray intensity on target. It is this phenomenon which is thought to make indirectly driven shock ignition experiments unfeasible [31] although a recent study showed these fast rises may be achievable [32]. This is another area in which burn-through barriers could potentially assist.

In the present study, a number of simulations have been performed to investigate how barrier design can modify the properties of X-rays reaching a target from a given radiation source. Firstly, 1-D radiation hydrodynamics simulations show how the choice of barrier material and composition are able to shape the temporal profile of the X-rays reaching a target. Then the adjustment of the

illumination uniformity at a spherical target surface is considered using a combination of 1-D radiation hydrodynamics simulations and a 3-D view-factor code.

X-RAY BURN-THROUGH

In this section a brief discussion is given of the radiation transport of X-ray heat waves and how the physics can inform barrier design. When high-intensity X-rays are incident on a material, they heat and ionise a surface layer of the material. The ionisation will reduce the opacity in that layer, thus allowing the X-rays to propagate further in. From there, the speed of the heat front relative to the hydrodynamic response of the material is dependent on the intensity of the radiation and the properties of the material. In general the heat front will propagate either supersonically or subsonically with respect to the heated material. In the supersonic case the heat front moves through the material above the speed of sound of the heated material and is trailed by a rarefaction wave which moves at the local sound speed. Alternatively, if the incident radiative heat flux is lower, or the material is denser or more opaque, the heat front propagates subsonically and the steep pressure gradient that forms induces a shock wave. This shock wave moves ahead of the heat front into the cold material. Heating may also start off supersonic but rapidly transition to subsonic behaviour in the case that the material is significantly opaque to the drive.

In low-Z materials (e.g. beryllium) the material may become relatively transparent to the drive upon heating due to it being largely stripped of bound electrons. In this case, the photons can freely propagate up to regions of high density. The system can be modelled as a steady state ablation [34] in which the ablative blow-off is completely transparent to incoming radiation and energy is entirely deposited at the ablation front. Here the transition between the sub- and super-sonic regimes will occur at a critical temperature, T_{crit} [35] given by

$$T_{\text{crit}} \approx \left(\frac{4\rho}{\sigma} \right)^{2/5} \left(\frac{R}{\mu} \right)^{3/5} \quad (1)$$

where ρ is solid density, σ is the Stefan-Boltzmann constant, R is the ideal gas constant and μ is the ionised molecular weight $\mu = A/(Z+1)$. Equation 1 predicts the T_{crit} values for beryllium, aluminium, copper and gold to be 380 eV, 424 eV, 647 eV and 805 eV respectively.

The case for high-Z materials (e.g. gold) differs in that the pre-plasma blow-off region is optically thick. In this case, the radiation can no longer penetrate directly to the heat front and instead is transported diffusively. These diffusive heat waves are often referred to as Marshak waves [36] and may be considered analytically by seeking self-similar solutions through dimensional analysis [37–39]. Marshak waves moving supersonically travel through

a material such that the penetration distance, x_p is given by [33]

$$x_p = \left(\frac{8\sigma T_0^4}{3k^{(R)}\rho\epsilon_0} t \right)^{1/2}, \quad (2)$$

where t is time, T_0 is the temperature at the source boundary, $k^{(R)}$ is the Rosseland mean opacity and ϵ_0 is the specific energy (density and specific energy are assumed to be constant as there is no hydrodynamic motion in the limit of extreme supersonic behaviour). Equation 2 actually somewhat over-predicts the penetration distance. Numerical simulations from reference 37 found that the penetration in gold is more accurately given by

$$x_p^2 = 2.96 \times 10^{-9} T_R^{-1.6} \int T_R^{5.5} dt, \quad (3)$$

where T_R is the time dependent boundary temperature. For a constant 314 eV source, after 1 ns equation 3 predicts the penetration distance to be 0.5 μm . Notice that, for a constant T_R , both equation 2 and 3 predict the penetration depth increases with \sqrt{t} . The result is that the speed of the heat front will slow with time. The supersonic phase will last whilst the speed of the heat front stays above the isothermal sound speed. From then on, the subsonic phase will begin and a shock front will overtake the heat front.

The above descriptions outline some idealised manifestations of heat-front propagation, however in practice the behaviour can be more nuanced due to the effects of ionisation, opacity and variations in the incident flux. Here the discussion is limited to two X-ray burn-through scenarios that are directly relevant to the simulations presented in this study. Firstly that of a weak shock wave with a significant radiative pre-cursor in a low-Z material. Note that here the precursor is not induced by shock heating, but by permeation of radiation from the X-ray drive through the shock front. In this case, the radiation drive sets up a shock front which does not reach sufficient density to become opaque to the incident flux. The material ahead of the shock is optically thin so radiation from the high temperature region is able to transport (non-diffusively) to the rear surface of the barrier. As the rear surface is heated it begins to expand and a rarefaction wave propagates back into the denser material. In this way the flux through the barrier increases as the length of the transmissive region ahead of the shock front decreases. Eventually the shock wave meets the rarefaction wave and the barrier begins to disassemble. After this point the flux through the barrier increases less rapidly as it continues to expand. This gives the total flux through the barrier against time a characteristic sigmoid shape (see figure 2). The second burn-through scenario that we shall describe is that of an ablatively driven shock wave in a mid- to high-Z material. In this case the ablation is subsonic and a strong shock-wave is

set-up, the compressed material so created prevents the radiation reaching the rear surface of the barrier. Note that this will be true regardless of the optical thickness of the material ahead of the shock front. The shock wave will propagate through the barrier and eventually will reach the rear surface resulting in disassembly. The result is a very low flux at the rear surface followed by a sharp and sudden rise. This is then followed by an increasingly gradual rise in flux as the plasma expands. Both of these two burn-through processes are observed in the simulation results presented in the next section. The weak shock front with radiative pre-cursor is seen in beryllium barriers and the ablatively driven shock front in aluminium, copper and gold.

TEMPORAL CONTROL

This section outlines the way in which burn-through barrier design can be adapted to modify the temporal profile of an X-rays source. Initially single material barriers were simulated for a range of thicknesses, and then more sophisticated copper-plastic barriers were studied. The simulations in this study used the one-dimensional Lagrangian radiation hydrodynamics code HYADES [40]. A number of different barriers were irradiated with a constant flux of Planckian X-rays equal to $1.0 \times 10^{15} \text{ W cm}^{-2}$, which is equivalent to a radiation temperature of 314 eV. In each simulation, the X-ray boundary emission from the rear surface of the barrier was monitored.

The simulations used multi-group radiation diffusion and SESAME [41] equations of state. Electron conduction is handled using a flux-limited diffusion model. The multi-group optical absorption coefficients employed are generated using the APOP [40] (Atomic Physics and Opacity Package) as follows: based on the conditions in each cell, at each time-point, a screened hydrogenic LTE model [42] is invoked. Thus, the ions and electrons in a given cell are characterized by a single kinetic temperature, T . This assumption permits the use of the steady-state Boltzmann-Saha equations on a cell-by-cell basis, at each time-point, which are functions only of the elemental composition, mass density, and temperature. The essential components of the model are 1) a screening theory, based on a WKB calculation, which gives the electron energy-levels as a function of the shell populations, 2) a Hartree-Fock approximation, which replaces the shell populations by their averages, and 3) LTE equations to determine the average shell-populations.

Once the bound-level populations and their energies are determined, along with the free electron density, the frequency-dependent opacities are found. For each prescribed radiation frequency band (photon group) there are free-free, bound-free, and bound-bound contributions. The bound-bound values are based on the Ein-

stein coefficients for spontaneous emission (the A coefficients), absorption, and stimulated emission (the two B coefficients). The bound-bound emission and absorption coefficients can then be calculated. The bound-free quantities are based on the Einstein-Milne relations which are the generalization of the Einstein coefficients to the continuum states. Again, the spontaneous and stimulated probabilities calculated from which the emission and absorption coefficients are found; a quantum mechanical correction in the form of so-called Gaunt factors is included. The free-free quantities are determined from considering the radiation emitted by an electron moving in a Coulomb field; again, a separate Gaunt factor is employed. Full details of these calculations can be found in reference 33. It is not expected, particularly in the case of high-Z materials, that the resultant opacities will be highly accurate. For the purpose of this study however, which is to demonstrate the functioning and utility of X-ray burn-through barriers, the errors so introduced are not critical. Where a burn-through barrier is to be employed for a particular application, the best available opacity data should be employed in its design.

The simulations of all the barriers in this study used the same uniform 314 eV X-ray source. In some cases, it may be that the X-ray source incident on the barrier has a strong time dependence (e.g. pulsed power sources). In this case, given that the source stays below the point of sub/supersonic transition, a strong shock front will still be set-up that holds back the radiation. However, the fluid dynamics may vary somewhat with the potential for the launching of multiple shocks. Under these conditions the barrier design would need to be adapted accordingly. From here it is shown that there is a lot of freedom in barrier design through which temporal control can be achieved.

An initial parameter scan was carried out for a number of materials to find how the burn-through properties differed. Shown here are the results for 15 μm of gold, 30 μm of copper and 800 μm of beryllium. Figure 2 shows the wide range of control that can be achieved over the temporal profile. The choice of material affects the start of the burn-through rise, the rate of the burn-through rise as well as the total flux that burns through the barrier. It can be seen that beryllium exhibits a higher initial flux and a more gradual rise. This is due to the fact that 314 eV is above the critical temperature for supersonic behaviour in beryllium. This means no shock front builds up to hold back the radiation. The explanation for this was outlined in detail in the previous section.

To investigate the effects of barrier thickness on burn-through properties, a number of simulations were run for aluminium, beryllium, copper and gold barriers. For each simulation the burn-through start time (point at which the initial rise occurs) the maximum burn-through flux, F_{max} (flux at $t = 15$ ns) and maximum burn-through rise rate, $(dF/dt)_{max}$ (maximum value of the derivative of

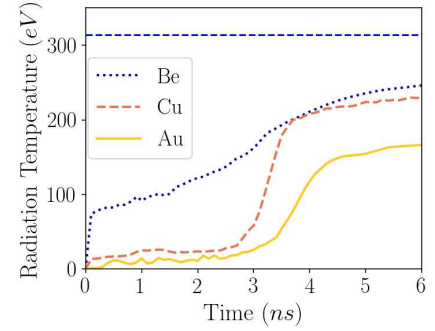


FIG. 2: Graph showing the rear surface X-ray burn-through profile for 15 μm gold, 30 μm copper and 800 μm beryllium. The blue dotted line shows the X-ray drive source temperature

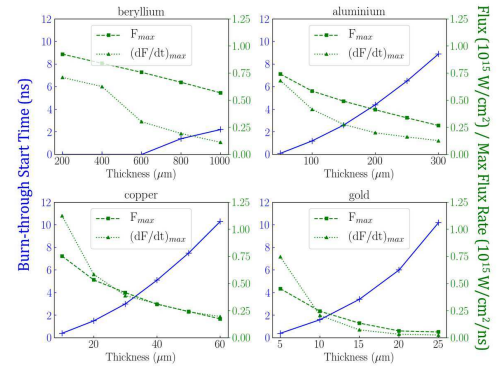


FIG. 3: Results of increasing thickness on burn-through properties. Start times are shown in blue, fluxes and maximum flux rates are shown in green, dotted lines act as visual aids.

the flux) were extracted. Figure 3 shows that increasing the barrier thickness will delay the burn-through start time and decrease the burn-through flux. These results show a simple way to adapt the pulse shape of the X-rays but more sophisticated barrier designs could help attain further control. For example, in some cases it may be desirable to achieve a significant delay in rise time whilst keeping a sharp rise and without greatly reducing the transmission of X-rays through the barrier. This is here achieved by placing a layer of mid-Z copper on the front of a low-Z plastic layer. The ablation of the copper occurs sub-sonically allowing a shock front to develop, then

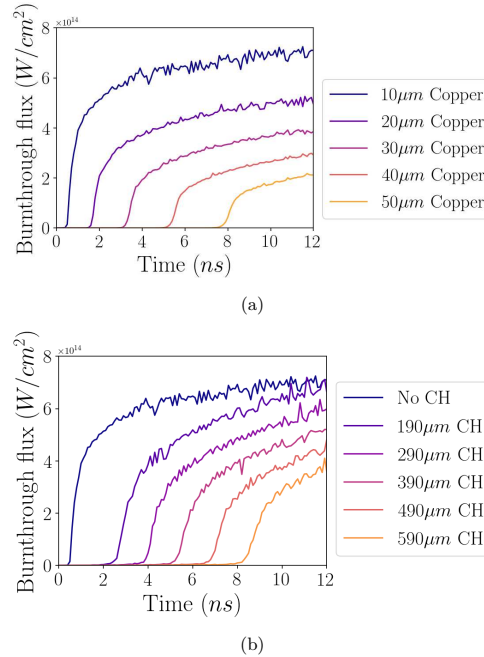


FIG. 4: Simulation results of the burn-through of (a) Five copper barriers of different thickness, (b) Five copper-plastic barriers with 10 μm of copper and varying thickness of plastic

the low-Z material acts as a medium for the shock front to propagate through, delaying the shock breakout and disassembly of the barrier. The shock breakout time can be controlled via the thickness of the lower opacity low-Z material. In this manner, the commencement of burn-through can be pushed back in time without significantly increasing the total opacity of the barrier. Figure 4 shows simulation results that compares the performance of copper and copper-plastic barriers of varying thickness, each driven by the same 314 eV source as before.

It can clearly be seen that the copper-plastic barrier is able to delay the burn-through rise with a less significant drop-off in burn-through flux intensity. The use of two materials in a burn-through barrier gives an extra element of control over the temporal profile. By varying the thicknesses of the two materials, one can control the total flux through the barrier and the delay in burn-through.

It is suggested that the use of a barrier that is subdivided into a significant number of smaller regions with different burn-through properties could be considered to

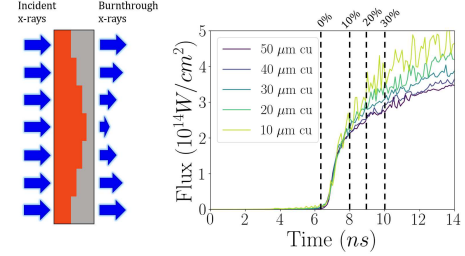


FIG. 5: A diagram illustrating the spatially varying barrier concept. A higher amount of mid-Z material at the centre of the barrier reduces the radiation intensity relative to the outer regions. Graphs showing the simulation results of 5 copper-plastic barriers designed so that the burn-through occurred simultaneously.

enable the development of complex temporal profiles. Such a pixelated barrier could potentially be used to control both spatial and temporal illumination simultaneously, and would not be beyond the capabilities of modern target fabrication facilities. Clearly though such a barrier would introduce additional concerns, with the potential for shear flows and instability growth within the barrier. In particular the Richtmyer-Meshkov [43] instability can seed growth for the Rayleigh-Taylor [44] instability at interfaces of discontinuous density. Such instabilities can cause mixing of the two materials and have been shown to be important in laser driven burn-through experiments [13, 45]. These effects are not considered further in this study and left as an area of possible future work.

SPATIAL CONTROL

The previous section demonstrated that temporal control over an X-ray source can be achieved in radiation-hydrodynamic simulations using an X-ray burn-through barrier. It is also possible to consider the use of these methods to design a barrier that introduces an intentional spatial perturbation in an initially isotropic radiation flux more uniform. Here we shall consider the former case. Taking the example of the copper-plastic barrier described above, it is possible to use sections of differing copper:plastic thickness ratio to change the spatial profile of the X-ray drive. Figure 5 shows a schematic diagram of such a barrier. The higher amount of copper near the centre reduces the intensity of the X-rays from that region of the barrier. Figure 5 shows the burn-through of 5 different barriers, designed such that the burn-through rise occurs at the same time. The thick-

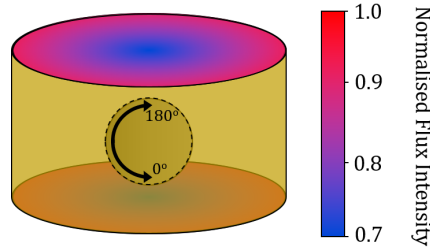


FIG. 6: A diagram of a viewfactor simulation. Burn-through sources that vary by 30% from centre to outer radius are shown at the top and bottom of the hohlraum.

ness of copper and plastic used in each the five barrier designs were $10\text{ }\mu\text{m}:500\text{ }\mu\text{m}$, $20\text{ }\mu\text{m}:320\text{ }\mu\text{m}$, $30\text{ }\mu\text{m}:205\text{ }\mu\text{m}$, $40\text{ }\mu\text{m}:115\text{ }\mu\text{m}$, and $50\text{ }\mu\text{m}:35\text{ }\mu\text{m}$. These different barrier designs could be incorporated into a single barrier so as to act in parallel with one another. When irradiated with an isotropic X-ray source, this would result in single burst of X-rays from the rear surface with a contrived spatial profile.

A 3-D view-factor code was used to investigate how a barrier with a spatial variation in its properties can be integrated with a hohlraum to adjust the drive symmetry at the surface of a spherical target. The view-factor code simulates complex hohlraum geometries by considering the radiation absorbed and emitted by a number of surface elements, calculating the remission based upon the wall albedo. The simulations used a 10 mm radius by 15 mm length cylindrical hohlraum with a wall albedo of 0.9, which is a reasonable approximation for a high-temperature gold hohlraum [46]. The burn-through barriers were mocked up by introducing spatially and temporally tailored X-ray emitting surfaces at either end of the cylindrical hohlraum. The output of these surfaces was based upon the radiation-hydrodynamics simulations described above. A 2.5 mm radius spherical surface with negligible albedo was placed inside the hohlraum so that the uniformity of the flux absorbed by the capsule could be monitored. A schematic of the simulation is shown in figure 6.

The burn-through barrier source shown in figure 5 was simulated using a number static view-factor simulations. It is noted that this is a simplified approach to modelling the time dependence. Effects such as time dependent albedos and the drop in temperature of the external chamber when burn-through occurs have been neglected. Here it has been assumed that the radiation field in the hohlraum cavity equilibrates on much faster timescales than the variation in the burn-through rear surface flux profile. This is valid as the transport of a photon from

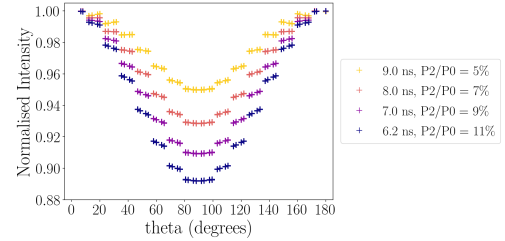


FIG. 7: The angular drive profiles incident on the capsule for the each snapshot of the burn-through source from figure 5. $\theta = 0^\circ$ and $\theta = 180^\circ$ are the points of the capsule closest to the source as seen in figure 6.

one end of the hohlraum to the other is on the order of 10s of picoseconds whereas the source intensity changes on nanosecond timescales. It is shown on figure 5 snapshots in time in which the variation across the barrier would be at 0% 10%, 20%, 30%. The variation in figure 5 reaches a maximum of 30% at 10 ns and remains so until the end. For each of these variations a view-factor calculation was carried out by defining a source that linearly varies from the centre to the outer radius by each of those amounts. The results of this view-factor calculation then represents what the radiation field will look like in the hohlraum cavity at that time. Figure 7 shows how the radiation field at each point in time mapped onto the spherical payload surface. It can be seen how as the spatial profile of the drive source changes in time, the flux distribution across the capsule is modified. At 6.2 ns when the source is uniform, there is a significant drive asymmetry due to the fact that poles of the capsule are nearer the source and therefore see much more flux. This gives rise to a P_2/P_0 variation of 11% where P_n is the corresponding Legendre polynomial. As the burn-through occurs, more radiation is shifted to the outer edge of the source. The capsule equator will see more flux and the angular flux profile begins to flatten. At 10 ns, where the variation of flux across the source is 30%, the P_2/P_0 variation has dropped to 5%. Further viewfactor simulations showed that a source that varied from 60% to 100% flux quadratically (instead of linearly) could reduce this the P_2/P_0 asymmetry to 1.4%. As with the spatial control simulations, it was assumed that the X-ray source on the front surface of the barrier was constant in time. As discussed before for temporally varying sources, the barrier design will need to be modified to account for the different shock dynamics.

It is noted here that the effect of this spatial drive-shaping on the capsule is highly dependent on the hohlraum geometry. Another set of simulations were run with more narrow hohlraum geometry, 2.55 mm radius by 8.2 mm length. In this case a 40% variation in the

source profile only yielded a 2% variation in the P_2/P_0 capsule asymmetry.

CONCLUSION

A technique for controlling X-ray flux in hohlraums using burn-through barriers has been demonstrated using a combination of 1-D radiation-hydrodynamics simulations and 3-D viewfactor calculations. It was shown how a uniform X-ray source can be modified in both time and space through barrier design. The temporal profile of the X-ray source can be shaped through choice of material and barrier thickness. A number of simulations of copper-plastic barriers showed how complex barrier design could allow for customisable pulse shaping. Further development of this concept showed how a copper-plastic burn-through barrier can be designed to create a single burst of spatially shaped X-ray radiation. A 3-D viewfactor code was then used to show how such a source could change the flux profile onto a payload mounted inside a hohlraum.

Burn-through barriers may give an extra degree of control to the target designer in addition to that which can be achieved through drive pulse shaping and hohlraum geometry modification. Here only a copper-plastic barrier was explored in any depth, however there is clearly scope for many other materials to be employed in such barriers, and a range of ways in which such barriers could potentially be combined to achieve interesting results. It is hoped that this work will be of interest particularly for modifying pulsed-power driven X-ray sources and for laser facilities that have a relatively limited number of beams and/or limited pulse-shaping capability.

ACKNOWLEDGEMENTS

The authors would like to thank R. Trines and R. Scott and the Rutherford Appleton Laboratory for providing access to and maintaining the computing systems on which HYADES was used. The authors would like to acknowledge the assistance of Jon Larsen of Cascade Applied Sciences in preparing the description of the APOP. This work was supported by the Engineering and Physical Sciences Research Council [EP/L01663X/1].

DATA AVAILABILITY

The data that support the findings of this study are available from the corresponding author upon reasonable request

- [1] V. N. Goncharov, O. V. Gotchev, E. Vianello, T. R. Boehly, J. P. Knauer, P. W. McKenty, P. B. Radha, S. P. Regan, T. C. Sangster, S. Skupsky, et al., *Phys. Plasmas* 13, 012702 (2006).
- [2] J. Lindl, O. Landen, J. Edwards, E. Moses, and NIC Team, *Phys. Plasmas* 21, 020501 (2014).
- [3] R. H. H. Scott, D. S. Clark, D. K. Bradley, D. A. Callahan, M. J. Edwards, S. W. Haan, O. S. Jones, B. K. Spears, M. M. Marinak, R. P. J. Town, et al., *Phys. Rev. Lett.* 110, 075001 (2013).
- [4] B. K. Spears, M. J. Edwards, S. Hatchett, J. Kilkenny, J. Knauer, A. Kritcher, J. Lindl, D. Munro, P. Patel, H. F. Robey, and R. P. J. Town, *Phys. Plasmas* 21, 042702 (2014).
- [5] J. E. Bailey, G. A. Rochau, R. C. Mancini, C. A. Iglesias, J. J. MacFarlane, I. E. Golovkin, C. Blancard, Ph. Cosse and G. Faussurier, *Phys. Plasmas* 16, 058101 (2009).
- [6] J. E. Bailey, T. Nagayama, G. P. Loisel, G. A. Rochau, C. Blancard, J. Colgan, Ph. Cosse, G. Faussurier, C. J. Fontes, F. Gilleron, et al., *Nature* 517, 56-59 (2015).
- [7] R. Cauble, D. W. Phillion, T. J. Hoover, N. C. Holmes, J. D. Kilkenny and R. W. Lee, *Phys. Rev. Lett.* 70, pp. 2102-2105 (1993).
- [8] H. S. Park, R. E. Rudd, R. M. Cavallo, N. R. Barton, A. Arsenlis, J. L. Belof, K. J. M. Blobaum, B. S. El-Dasher, J. N. Florando, C. M. Huntington, et al., *Phys. Rev. Lett.* 114, 065502 (2015).
- [9] S. D. Rothman, A. M. Evans, C. J. Horsfield, P. Graham and B. R. Thomas, *Phys. Plasmas* 9, 1721 (2002).
- [10] R. F. Smith, J. H. Eggert, R. Jeanloz, T. S. Duffy, D. G. Braun, J. R. Patterson, R. R. Rudd, J. Biener, A. E. Lazicki, A. V. Hamza, et al., *Nature* 511, 330-333 (2014).
- [11] S. Zhang, B. Militzer, M. C. Gregor, K. Caspersen, L. H. Yang, J. Gaffney, T. Ogitsu, D. Swift, A. Lazicki, D. Erskine, et al., *Phys. Rev. E* 98, 023205 (2018).
- [12] J. W. Murdoch, J. D. Kilkenny, D. R. Gray and W. T. Toner, *Phys. Fluids* 24, 2107 (1981).
- [13] J. Delettret, D. K. Bradley, P. A. Jaanimagi and C. P. Verdon, *Phys. Rev. A* 41, pp. 5583-5593 (1990).
- [14] J. Edwards, M. Dunne, D. Riley, R. Taylor, O. Willi and S. J. Rose, *Phys. Rev. Lett.* 67, pp. 3780-3783 (1991).
- [15] D. R. Kania, H. Kornblum, B. A. Hammel, J. Seely, C. Brown, U. Feldman, G. Glendinning, P. Young, E. Hsieh, M. Hennesian, et al., *Phys. Rev. A* 46, pp. 7853-7868 (1992).
- [16] W. Schwanda and K. Eidmann, *Phys. Rev. Lett.* 69, pp. 3507-3510 (1992).
- [17] C. A. Back, L. Da. Silva, H. Kornblum, D. Montgomery, B. Macgowan, G. Glendinning, J. Fenske, E. Hsieh, and R. W. Lee, *J. Quant. Spectrosc. Radiat. Transfer* 51, No 1 2, pp. 19-25 (1994).
- [18] R. E. Olson, G. A. Rochau, O. L. Landen, and R. J. Leeper, *Phys. Plasmas* 11, 2778 (2004).
- [19] R. E. Olson, R. J. Leeper, S. C. Dropinski, L. P. Mix, G. A. Rochau, S. H. Glenzer, O. S. Jones, L. J. Suter, J. L. Kaae, C. H. Shearer, and J. N. Smith, *Rev. Sci. Instrum.* 74, 2186 (2003).
- [20] J. Lindl, *Phys. Plasmas* 2 (11), pp. 3933-4024 (1995).
- [21] M. D. Rosen, *Phys. Plasmas* 3, 1803 (1996).
- [22] J. H. Hammer, M. Tabak, S. C. Wilks, J. D. Lindl, D. S. Bailey, P. W. Rambo, A. Toor, G. B. Zimmerman, and

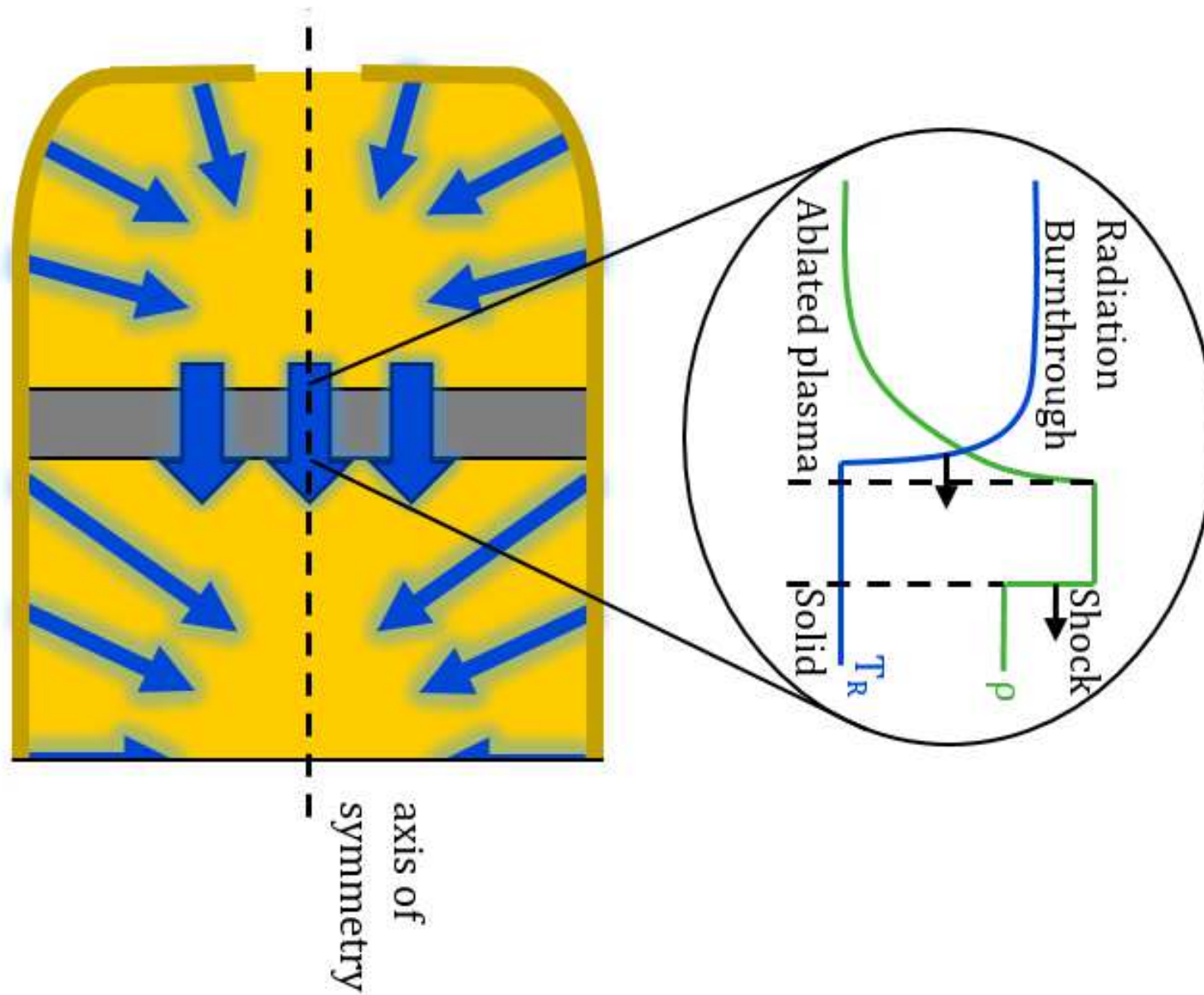
This is the author's peer reviewed, accepted manuscript. However, the online version of record will be different from this version once it has been copyedited and typeset.

PLEASE CITE THIS ARTICLE AS DOI: 10.1063/5.0014798

- [23] J. L. Porter, Phys. Plasmas 6, 2129 (1999).
- [24] M. E. Cuneo, R. A. Vesey, J. L. Porter, G. R. Bennett, D. L. Hanson, L. E. Ruggles, W. W. Simpson, G. C. Idzorek, W. A. Stygar, J. H. Hammer, et al., Phys. Rev. Lett. 88, 4 (2002).
- [25] M. E. Cuneo, R. A. Vesey, G. R. Bennett, D. B. Sinars, W. A. Stygar, E. M. Waisman, J. L. Porter, P. K. Rambo, I. C. Smith, S. V. Lebedev, et al., Plasma Phys. Control. Fusion 48, R1 (2006).
- [26] T. W. L. Sanford, R. E. Olson, R. L. Bowers, G. A. Chandler, M. S. Derzon, D. E. Hebron, R. J. Leeper, R. C. Mock, T. J. Nash, D. L. Peterson, et al., Phys. Rev. Lett. 83, pp. 5511-5514 (1999).
- [27] G. H. Miller, E. I. Moses, and C. R. Wuest, Opt. Eng. (Bellingham) 43, 2841 (2004).
- [28] E. L. Dewald, R. Tommasini, N. B. Meezan, O. L. Landen, S. Khan, R. Rygg, J. Field, A. S. Moore, D. Sayre, A. J. MacKinnon, et al., Phys. Plasmas 25, 092702 (2018).
- [29] E. L. Dewald, C. Thomas, S. Hunter, L. Divol, N. Meezan, S. H. Glenzer, L. J. Suter, E. Bond, J. L. Kline, J. Celeste, et al., Rev. Sci. Instrum., 81 (10) (2010).
- [30] T. Döppner, C. A. Thomas, L. Divol, E. L. Dewald, P. M. Celliers, D. K. Bradley, D. A. Callahan, S. N. Dixit, J. A. Harte, S. M. Glenn, et al., Phys. Rev. Lett., 108 (13), 135006 (2012).
- [31] E. L. Dewald, F. Hartemann, P. Michel, J. Milovich, M. Hohenberger, A. Pak, O. L. Landen, L. Divol, H. F. Robey, O. A. Hurricane, et al., Phys. Rev. Lett., 116 (7), 075003 (2016).
- [32] L. J. Perkins, R. Betti, K. N. Lafortune, and W. H. Williams, Phys. Rev. Lett. 103, 045004 (2009).
- [33] W. Trickey, and J. Pasley, Plasma Phys. Control. Fusion 61, 105010 (2019).
- [34] J. Larsen, "Foundations of high-energy-density physics: physical processes of matter at extreme conditions." (Cambridge University Press, 2017).
- [35] S. Atzeni and J. Meyer-Ter-Vehn, The Physics of Inertial Fusion (Oxford University Press, 2004).
- [36] 'Ablation gas dynamics of low-Z materials illuminated by soft X-rays', S. Hatchett, pub. by Lawrence Livermore National Laboratory, UCRL-JC-108348, (1991)
- [37] R. E. Marshak, Phys. Fluids 1, 24 (1958).
- [38] J. H. Hammer and M. D. Rosen, Phys. Plasmas 10, 1829, (2003).
- [39] R. Pakula and R. Sigel, Phys. Fluids 28, 232 (1985)
- [40] Ya. B. Zel'dovich and Yu. P. Raizer, Physics of Shock Waves and High Temperature Hydrodynamic Phenomena (Academic, New York, 1966)
- [41] HYADES and APOP commercial products of Cascade Applied Sciences email larsen@casinc.com.
- [42] See National Technical Information Service Document No. LA7130 (B. I. Bennett, J. D. Johnson, G. I. Kerley, and G. T. Rood, "Recent development in the SESAME equation-of-state library", Los Alamos National Laboratory, Los Alamos, NM, LA-7130, 1978). Copies may be obtained from the National Technical Information Service, Springfield, VA 22161.
- [43] R. M. More, J. Quant. Spectrosc. Radiat. Transfer 27, No 3, pp. 345-357 (1982).
- [44] E. E. Meshkov, Fluid Dynamics 4.5, 101-104 (1969).
- [45] D. E. Sharp, Physica D 12, 3 (1983).
- [46] J. Delettrez, D. K. Bradley, and C. P. Verdon, Phys. Plasmas 1, 2342 (1994).
- [47] L. J. Suter, R. L. Kauffman, C. B. Darrow, A. A. Hauer, H. Kornblum, O. L. Landen, T. J. Orzechowski, D. W. Phillion, J. L. Porter, L. V. Powers, et al., Phys. Plasmas 3, 2057, (1996).

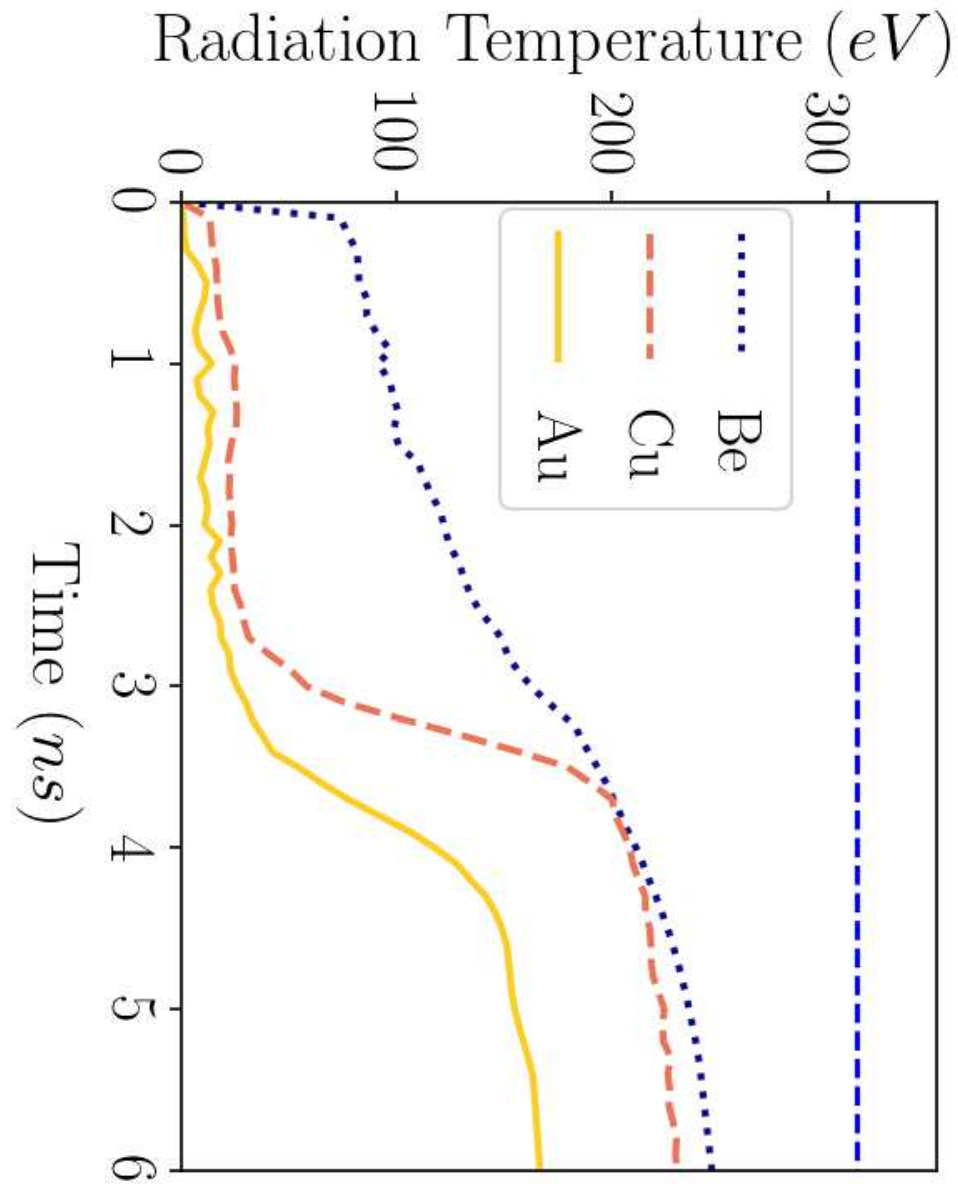
This is the author's peer reviewed, accepted manuscript. However, the online version of record will be different from this version once it has been copyedited and typeset.

PLEASE CITE THIS ARTICLE AS DOI: 10.1063/5.0014798



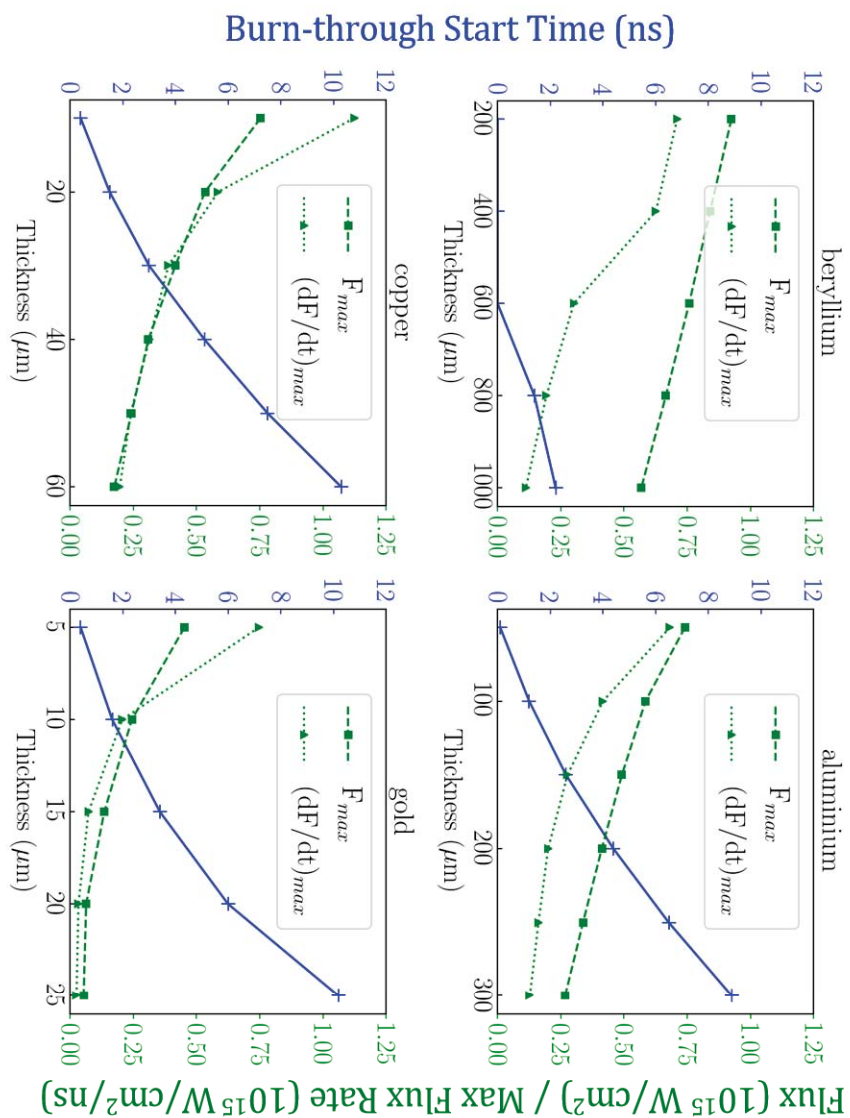
This is the author's peer reviewed, accepted manuscript. However, the online version of record will be different from this version once it has been copyedited and typeset.

PLEASE CITE THIS ARTICLE AS DOI: 10.1063/5.0014798



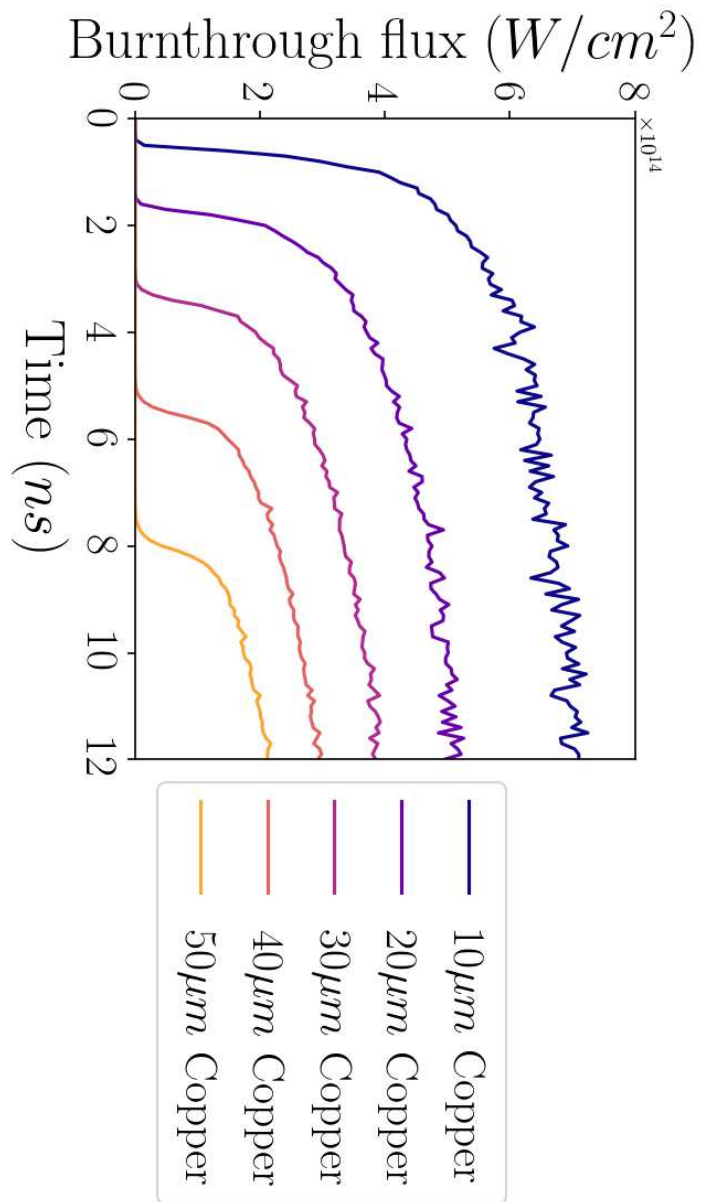
This is the author's peer reviewed, accepted manuscript. However, the online version of record will be different from this version once it has been copyedited and typeset.

PLEASE CITE THIS ARTICLE AS DOI: 10.1063/5.0014798



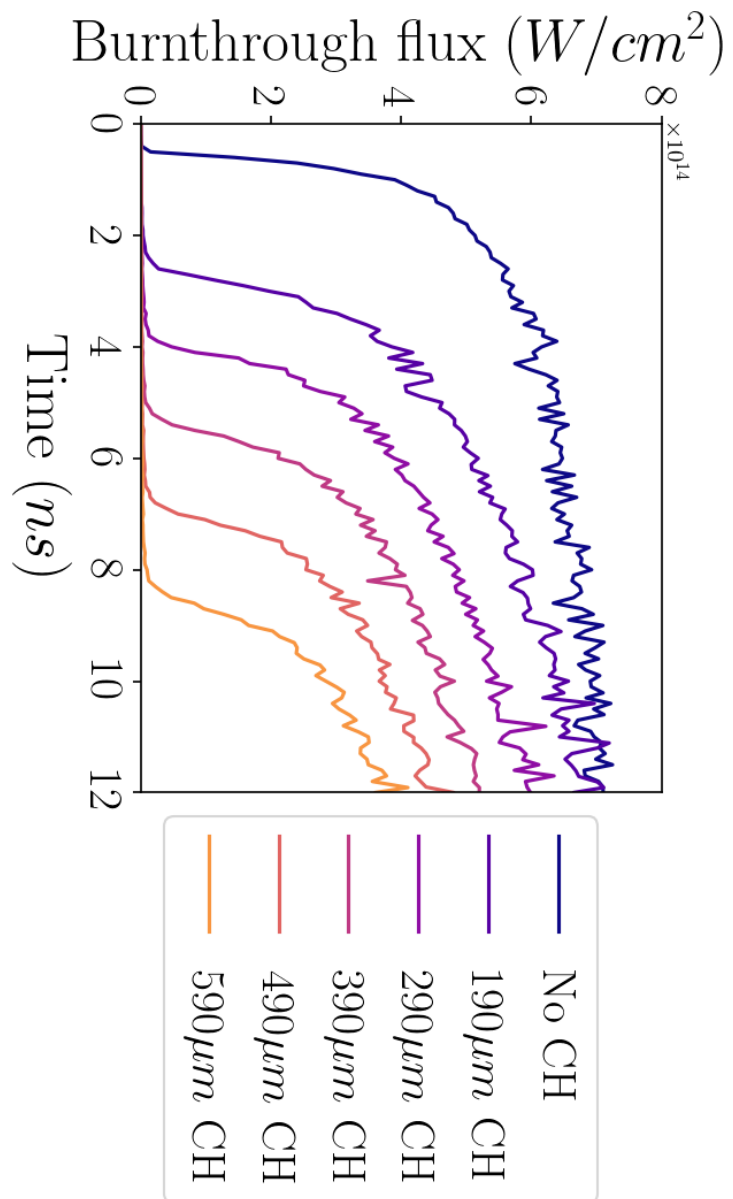
This is the author's peer reviewed, accepted manuscript. However, the online version of record will be different from this version once it has been copyedited and typeset.

PLEASE CITE THIS ARTICLE AS DOI: 10.1063/5.0014798



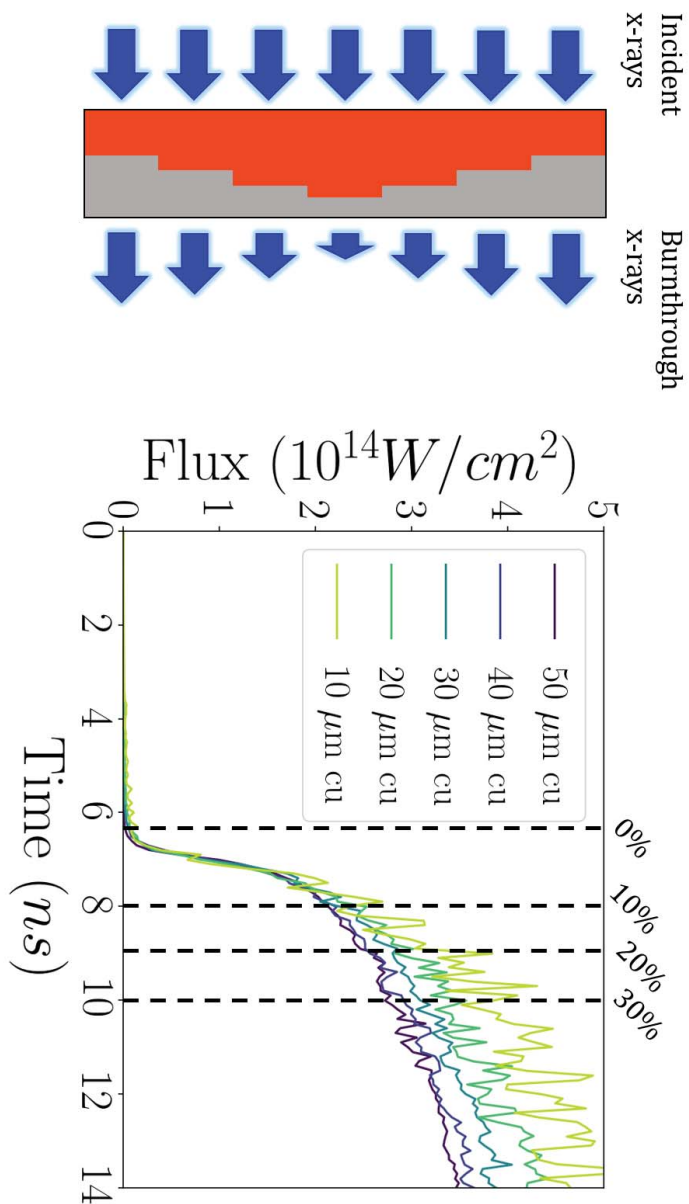
This is the author's peer reviewed, accepted manuscript. However, the online version of record will be different from this version once it has been copyedited and typeset.

PLEASE CITE THIS ARTICLE AS DOI: 10.1063/5.0014798



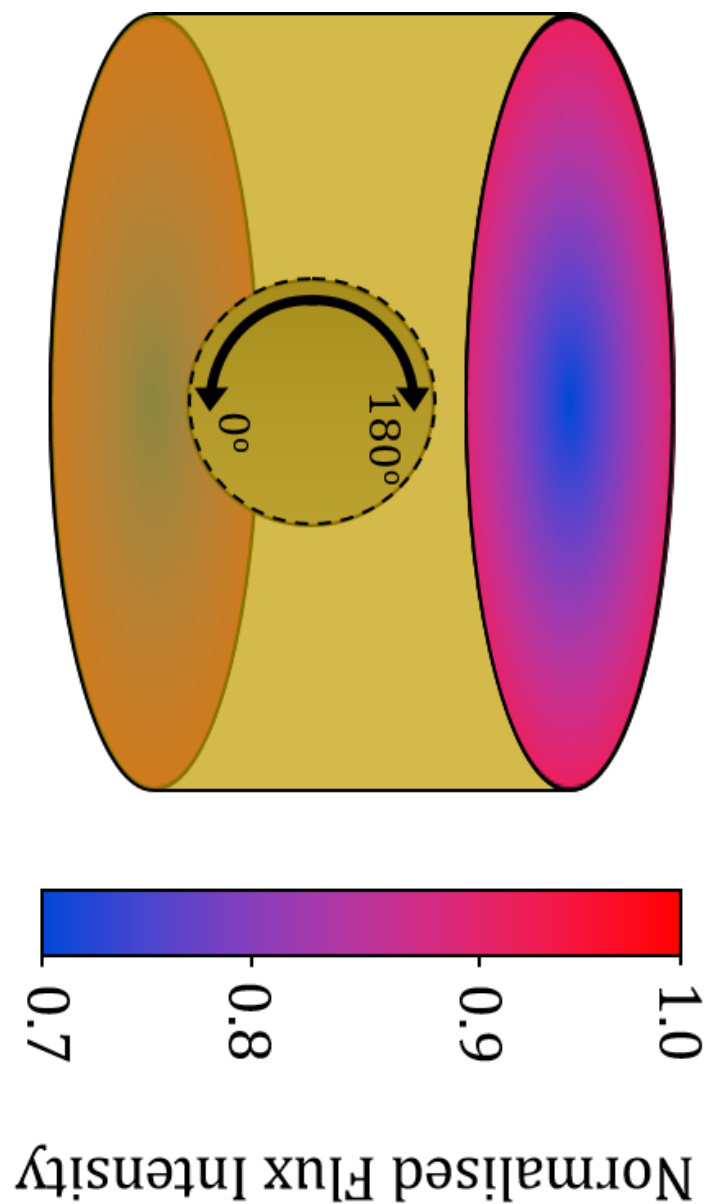
This is the author's peer reviewed, accepted manuscript. However, the online version of record will be different from this version once it has been copyedited and typeset.

PLEASE CITE THIS ARTICLE AS DOI: 10.1063/5.0014798



This is the author's peer reviewed, accepted manuscript. However, the online version of record will be different from this version once it has been copyedited and typeset.

PLEASE CITE THIS ARTICLE AS DOI: 10.1063/5.0014798



This is the author's peer reviewed, accepted manuscript. However, the online version of record will be different from this version once it has been copyedited and typeset.

PLEASE CITE THIS ARTICLE AS DOI: 10.1063/5.0014798

